Bearing-only Motional Target-Surrounding Control for Multiple Unmanned Surface Vessels

Bin-Bin Hu, Hai-Tao Zhang*, *Senior Member*, *IEEE*

***Abstract*—This paper proposes a distributed bearing-only controller for multiple unmanned surface vessels (USVs) to encircle and rotate evenly around a motional target with inter-USV topologies. The distributed control law consists of three terms, i.e., a bearing-only estimation term to approximate the target state, an upper level surrounding term to fulfill the target-surrounding mission, and single vessel regulation term to track the upper level signal. Significantly, technical conditions are derived to guarantee the asymptotical stability of the closed-loop system. Finally, experimental results on a real platform composed of three HUSTER-0.3 USVs and a target vessel are conducted to substantiate the effectiveness of the proposed controller.**

***Index Terms*—Collaborative control, target surrounding, bearing-only measurement, unmanned surface vessel.**

I. Introduction

In recent years, control of the unmanned surface vessels (USVs) has attracted increasing attention for their efficiency, flexibility and adaptivity to complex environments, which has application potential in trajectory tracking [1]–[5], path following [6]–[9], and collective exploration [10]–[14], etc. Target-surrounding mission by the cooperative multiple vessels has been playing an essential role in surveillance, conveyance, detection, saturation attack and escort formation, etc.

Notably, the research of USV target-surrounding problem originates from the scenario of multi-agent systems (MASs). Due to the theoretical challenges in such a problem, initial efforts were mostly devoted to the strategies depending on both position and velocity measurements. Chen & Ren *et al.* [15] developed an estimation-and-control framework with a fixed topology to enclose a cluster of stationary targets. Lan *et al.* [16] designed a hybrid control approach to address a static target surrounding problem. Afterwards, Liu & Chen *et al.* [17] proposed a hierarchical output regulation scheme to surround a static target. Chen [18] proposed a cooperative controller consisting of attractive, repulsive and rotation components to tackle a specific target fencing problem with guaranteed collision avoidance.

This work was supported by in part by the National Natural Science Foundation of China (NNSFC) under Grants U1713203, 51729501, 61673330, in part by the National Natural Science Foundation of Hubei Province under Grant 2019CFA005, in part by the Program for Core Technology Tackling Key Problems of Dongguan City under Grant 2019622101007, and in part by the Fundamental Research Funds for Central Universities, HUST: 2020JYCXJJ070. (*Corresponding author: H.-T. Zhang*).

B.-B. Hu, H.-T. Zhang are with the School of Artificial Intelligence and Automation, the Key Laboratory of Image Processing and Intelligent Control, and the State Key Lab of Digital Manufacturing Equipment and Technology, Huazhong University of Science and Technology, Wuhan 430074, China (email: hbb@hust.edu.cn; zht@mail.hust.edu.cn).

With the increasing complexity of the large volume of aquatic missions, more attention has been paid to the challenging scenarios to encircling motional targets. For instance, Guo *et al.* [19] proposed a distributed protocol merely depending on neighboring positions to surround a moving target. Yu & Liu proposed a distributed dynamic controller to enclose a moving target with fixed [20] and switching [21] direct inter-agent topologies, respectively. Afterwards, Shoja *et al.* [22] proposed an adaptive approach to tackle the surrounding problem for non-identical agents to encircle multiple motional targets. Unfortunately, the aforementioned works [19]–[22] only consider first-order MASs due to the arduousness in target-surrounding control for high-order MASs. To achieve more realistic missions, Shi *et al.* [23] afterwards investigated a second-order MAS target-surrounding problem with the assistance of Lasalle's Invariance principle [24]. Li *et al.* [25] presented a cooperative surrounding scheme with guaranteed collision avoidance for networked MASs with nonlinear Lagrangian dynamics. Hu *et al.* [26] designed a distributed equal-distance surrounding controller for second-order nonlinear MASs. Peng *et al.* [27] afterwards proposed an event-triggered dynamic surface controller for a USV to enclose a dynamic target. Xu [28] presented a novel fault tolerant control scheme for a group of USVs to track a target with only line-of-sight range and angle. Hu *et al.* [29] developed a distributed surrounding controller for multiple USVs with evenly varying interconnection topologies. Kou *et al.* [30] studied the moving-target-fencing problem of multiple second-order vehicles, where the target moves with an unknown constant velocity.

However, due to the high cost of onboard sensors, the position and velocity of the target are not always available for the USVs in practice. That motivates another research line merely with bearing measurements (bearing vectors or subtended bearing angles), which only requires comparably cheap sensors such as pin-hole cameras and wireless sensor arrays. As one of the pioneer works in this regard, Zheng *et al.* [31] developed a control scheme merely relying on local bearing measurements to ensure the enclosing of a stationary target. Li *et al.* [32] proposed a distributed bearing-only controller for a stationary target in a 3D space. Afterwards, Deghat *et al.* [33] investigated the problem of localization and circumnavigation of a moving target with an unknown velocity. Yang *et al.* [34] studied a target-entrapping problem merely by bearing measurements. Dou *et al.* [35] designed a distributed controller for the agents to enclose a motional target and achieve desirable collective patterns only with bearing measurements. Unfortunately, the aforementioned bearing-

This article has been accepted for publication in a future issue of this journal, but has not been fully edited. Content may change prior to final publication. Citation information: DOI 10.1109/TIE.2021.3076719, IEEE Transactions on Industrial Electronics

based works [31]–[35] still focus on the first-order MASs and have not considered more practical USV scenarios with severe nonlinearity and strong coupling dynamics. Although target-surrounding control with USV dynamics has been investigated via position-based information in [17], [26], [27], [29], [36], the theoretical issue for USV group control with bearing-only measurements still remains a dilemma [33]–[35].

Technically speaking, the main challenges lie in the existence of bounded errors, and partial availability of the target velocity to the USVs, which limit the further application of multi-USV cooperative control. This motivates us to propose a niche distributed motional target-surrounding protocol for multi-USV systems to govern the surrounding error to zero with bearing-only feedbacks.

Besides the capability of motional target surrounding for multi-USV systems, the proposed controller drives USVs to everlastingly rotate around the motional target vessel with time-changing topologies, which is indispensable for the asymptotic convergence of the bearing-only target estimation. Unlike the simulation-only verification of most of the existing works [32]–[35], experiments are conducted in this study with a real multi-USV platform consisting of a USV motion capturing system, a monitor station, three 3D-printed HUSTER-0.3 vessels and a target vessel to verify the proposed framework.

In brief, the contribution of the paper lies in proposing a distributed bearing-only controller for the multi-USV systems to collectively surround and rotate evenly around a motional target vessel, with the design of a bearing-only target estimator, an upper level surrounding protocol, and single vessel regulator.

The remainder of this paper is organized as follows. Section II formulates the problem. Section III provides the main technical result with rigorous mathematical proof. Experiments on a real multi-USV platform are conducted in Section IV. Finally, conclusion is drawn in Section V.

II. Problem Formulation

Throughout the paper, $\mathbb{R}$ and $\mathbb{R}^+$ denote the real number and positive real number, respectively. $\mathbb{R}^n$ denotes the n-dimensional Euclidean space, $\|*\|$ is the Euclidean norm of a vector $*$. $*^{-1}$ denotes the inversion of a square matrix $*$. $*^\intercal$ represents the transpose of a matrix $*$. $\int *(s)d(s)$ denotes the integral of a function $*$, $\otimes$ denotes Keroneck product.

Consider a multi-USV system consisting of n USVs, of which each is described by the kinematics in the Cartesian coordinates [37],

$$\begin{aligned}\dot{x}_i &= u_i \cos\psi_i - v_i \sin\psi_i,\\ \dot{y}_i &= u_i \sin\psi_i - v_i \cos\psi_i,\\ \dot{\psi}_i &= r_i,\end{aligned} \tag{1}$$

where $q_i(t) = [x_i(t), y_i(t)]^\intercal \in \mathbb{R}^2$ denotes the position, $\psi_i(t) \in \mathbb{R}$ the yaw angle of USV i, respectively, and $u_i(t), v_i(t), r_i(t) \in \mathbb{R}$ the surge, the sway and the yaw velocities of USV i in the USV coordinate, respectively.

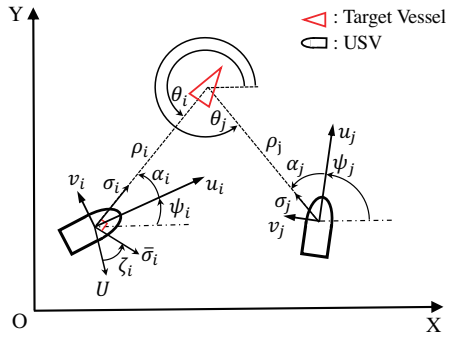

Fig. 1. Illustration of the bearing angle in the multi-USV system.

The dynamics of USV i generally follow a practical model (see e.g., [17]) as

$$\begin{aligned}\dot{u}_i &= k_1 u_i + k_2 v_i r_i + k_3 \tau_{i,1},\\ \dot{r}_i &= k_4 r_i + k_5 \tau_{i,2},\\ \dot{v}_i &= k_6 v_i + k_7 u_i r_i,\end{aligned} \tag{2}$$

where $k_1, k_2, k_3, k_4, k_5, k_6, k_7 \in \mathbb{R}$ are the identified parameters via zig-zag experiments afterwards, and $\tau_{i,1}, \tau_{i,2} \in \mathbb{R}$ the actuator inputs of USV i.

A motional target represented by $q_d(t) = [x_d(t), y_d(t)]^\intercal \in \mathbb{R}^2$ satisfies

$$\dot{q}_d = p_d \tag{3}$$

with a constant velocity $p_d = [v_x^d, v_y^d]^\intercal \in \mathbb{R}^2$.

As is shown in Fig. 1, it is assumed that only the relative bearing angle α_i is measured between the i-th USV and the target in the i-th USV's coordination frame, which is not necessarily aligned to the frames of the other USVs, but not the position q_d or the velocity p_d of the target vessel. Combined with the yaw angle ψ_i, one has

$$\sigma_i := \frac{q_{d,i}}{\|q_{d,i}\|} \tag{4}$$

as a unit vector with $\angle\sigma_i := \psi_i + \alpha_i$ and $q_{d,i} := q_d - q_i$ in Eq. (21).

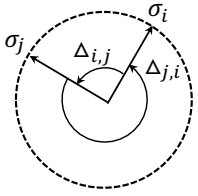

Fig. 2. Illustration of the forward and backward separation angles $\Delta_{i,j}$ and $\Delta_{j,i}$, respectively, between vector σ_i of USV i and vector σ_j of USV j.

In a multi-USV system, define the communication topology as $\mathcal{G}(\mathcal{V}, \mathcal{E})$, where $\mathcal{V} := \{1, 2, \ldots, n\}$ is the node set and $\mathcal{E} := \{(i,j), j \in \mathcal{N}_i, i \in \mathcal{V}\}$ the edge set. Here, $\mathcal{N}_i = \{j \in \mathcal{V} | \min_{j\neq i}\Delta_{i,j}, \min_{j\neq i}\Delta_{j,i}\}$ is the neighbor set of USV i, where $\Delta_{i,j} \in [0, 2\pi), i \neq j \in \mathcal{V}$, is the forward separation angle from USV i to USV j and measured by counterclockwisely rotating σ_i until coinciding with σ_j; and

This article has been accepted for publication in a future issue of this journal, but has not been fully edited. Content may change prior to final publication. Citation information: DOI 10.1109/TIE.2021.3076719, IEEE Transactions on Industrial Electronics

$\Delta_{j,i} \in [0, 2\pi), i \neq j \in \mathcal{V}$, the backward separation angle from USV j to USV i in Fig. 2 (see, e.g., [35]). Note that there might be more than two neighbors in $\mathcal{N}_i$, where the pre-neighbor i^+ and next-neighbor i^- of USV i can be selected randomly from $\mathcal{N}_i$, respectively.

Let the relative distance ρ_i and the bearing angle θ_i between the USV i and the target vessel be

$$\begin{aligned} \rho_i &= \sqrt{(x_i - x_d)^2 + (y_i - y_d)^2}, \\ \theta_i &= \text{arctan2}(y_i - y_d, x_i - x_d) + 2\kappa\pi \in [0, 2\pi) \end{aligned} \tag{5}$$

with an appropriately selected integer κ to make sure that $\theta \in [0, 2\pi)$. arctan2(y, x) denotes a two-argument arctangent function retuning the angle of vector (x, y) as a numeric value between $-\pi$ and π radians. Then, one has

$$\theta_i = \psi_i + \alpha_i + \pi \tag{6}$$

with α_i, ψ_i illustrated in Fig. 1. Define the separation angle ς_i between USV i and its pre-neighbor i^+ with respect to the target vessel as

$$\varsigma_i := \theta_{i^+} - \theta_i + \xi_i \tag{7}$$

with

$$\xi_i = \begin{cases} 0, & \theta_{i^+} - \theta_i \geq 0, \\ 2\pi, & \theta_{i^+} - \theta_i < 0. \end{cases}$$

With the target and neighboring information above, the following assumptions are necessary for afterwards derivation.

Assumption 1. *The velocity $p_d \in \mathbb{R}^2$ of the target in* (3) *has an upper bound $p_d^* \in \mathbb{R}^+$, i.e., $\|p_d\| \leq p_d^*$.*

Assumption 1 is reasonable since the energy of the target vessel is always limited in practice, which implies that the velocity of target has an upper bound.

Assumption 2. *Each USV $i \in \mathcal{V}$ satisfies $\mathcal{N}_i^c = \{i^+, i^-\}$ with $\mathcal{N}_i^c$ representing the communication neighbor set.*

Under Assumption 2, each USV has access to the pre-neighbor i^+ and next-neighbor i^- via inter-USV communication. The communication topology $\mathcal{G}(\mathcal{V}, \mathcal{E})$ depends on the minimal-neighbor strategy, which is always strongly connected [38] even for the time-changing neighbors. Thus, the topology is of low communication cost, which is desirable in real applications.

For further derivations, a definition of target surrounding is necessary as well.

Definition 1. *(Target surrounding) The USVs asymptotically surround a target vessel with the following properties as*

$$\lim_{t\to\infty} \rho_i(t) = \rho_d, \lim_{t\to\infty} \varsigma_i = \frac{2\pi}{n}, \tag{8}$$

where $\rho_d \in \mathbb{R}^+$ is the desired radius and ς_i the separation angle in (7)*.*

Definition 1 shows that all the USVs evenly surround the target vessel, which implies the target vessel is in the interior of a convex hull of the USVs [17], [18], i.e.,

$$\lim_{t\to\infty} P_{x_d(t)}(x(t)) = 0 \tag{9}$$

with $x := [x_1^\intercal, \ldots, x_n^\intercal]^\intercal$, $P_{x_d}(x) := \min_{s\in\text{co}(x)} \|x_d - s\|$ and

$$\text{co}(x) := \left\{ \sum_{i\in\mathcal{V}} \lambda_i x_i : \lambda_i \geq 0, \forall i \text{ and } \sum_{i\in\mathcal{V}} \lambda_i = 1 \right\}.$$

Then, take the temporal derivative of ρ_i along the trajectory of Eq. (5) as

$$\begin{aligned} \dot{\rho}_i &= \frac{(x_i - x_d)(\dot{x}_i - v_x^d) + (y_i - y_d)(\dot{y}_i - v_y^d)}{\sqrt{(x_i - x_d)^2 + (y_i - y_d)^2}} \\ &= \begin{bmatrix} \cos\theta_i & \sin\theta_i \end{bmatrix} \begin{bmatrix} \dot{x}_i - v_x^d \\ \dot{y}_i - v_y^d \end{bmatrix}. \end{aligned} \tag{10}$$

Analogously, the temporal derivative of θ_i along the trajectory of Eq. (5) is

$$\begin{aligned} \dot{\theta}_i &= \frac{(x_i - x_d)^2}{\rho_i^2} \frac{(x_i - x_d)(\dot{y}_i - v_y^d) - (y_i - y_d)(\dot{x}_i - v_x^d)}{(x_i - x_d)^2} \\ &= \frac{\begin{bmatrix} -\sin\theta_i & \cos\theta_i \end{bmatrix}}{\rho_i} \begin{bmatrix} \dot{x}_i - v_x^d \\ \dot{y}_i - v_y^d \end{bmatrix}. \end{aligned} \tag{11}$$

Eqs. (10) and (11) can be rewritten into a compact form as

$$\begin{bmatrix} \dot{\rho}_i \\ \rho_i\dot{\theta}_i \end{bmatrix} = \begin{bmatrix} \cos\theta_i & \sin\theta_i \\ -\sin\theta_i & \cos\theta_i \end{bmatrix} \begin{bmatrix} \dot{x}_i - v_x^d \\ \dot{y}_i - v_y^d \end{bmatrix}. \tag{12}$$

Direct calculation gives

$$\begin{bmatrix} \dot{x}_i \\ \dot{y}_i \end{bmatrix} = \begin{bmatrix} \cos(-\theta_i) & \sin(-\theta_i) \\ -\sin(-\theta_i) & \cos(-\theta_i) \end{bmatrix} \begin{bmatrix} \dot{\rho}_i \\ \rho_i\dot{\theta}_i \end{bmatrix} + \begin{bmatrix} v_x^d \\ v_y^d \end{bmatrix}. \tag{13}$$

It follows from Eq. (1) that

$$\begin{bmatrix} u_i \\ v_i \end{bmatrix} = \begin{bmatrix} \cos\psi_i & \sin\psi_i \\ -\sin\psi_i & \cos\psi_i \end{bmatrix} \begin{bmatrix} \dot{x}_i \\ \dot{y}_i \end{bmatrix}. \tag{14}$$

Substituting Eq. (13) into Eq. (14) yields

$$\begin{aligned} \begin{bmatrix} u_i \\ v_i \end{bmatrix} = &\begin{bmatrix} \cos(\psi_i - \theta_i) & \sin(\psi_i - \theta_i) \\ -\sin(\psi_i - \theta_i) & \cos(\psi_i - \theta_i) \end{bmatrix} \begin{bmatrix} \dot{\rho}_i \\ \rho_i\dot{\theta}_i \end{bmatrix} \\ &+ \begin{bmatrix} \cos\psi_i & \sin\psi_i \\ -\sin\psi_i & \cos\psi_i \end{bmatrix} \begin{bmatrix} v_x^d \\ v_y^d \end{bmatrix}. \end{aligned} \tag{15}$$

Using the fact $\psi_i - \theta_i = -\alpha_i - \pi$ in (6), one has

$$\begin{aligned} \begin{bmatrix} u_i \\ v_i \end{bmatrix} = &\begin{bmatrix} -\cos\alpha_i & \sin\alpha_i \\ -\sin\alpha_i & -\cos\alpha_i \end{bmatrix} \begin{bmatrix} \dot{\rho}_i \\ \rho_i\dot{\theta}_i \end{bmatrix} \\ &+ \begin{bmatrix} \cos\psi_i & \sin\psi_i \\ -\sin\psi_i & \cos\psi_i \end{bmatrix} \begin{bmatrix} v_x^d \\ v_y^d \end{bmatrix}. \end{aligned} \tag{16}$$

Let u_i^r, v_i^r be the upper level signals for u_i, v_i, respectively, in the kinematics (1). Define the signal errors as

$$\widetilde{u}_i := u_i - u_i^r, \widetilde{v}_i := v_i - v_i^r, \tag{17}$$

it thus follows from Eqs. (16) and (17) that the dynamics of ρ_i, θ_i can be formulated as

$$\begin{aligned} \begin{bmatrix} \dot{\rho}_i \\ \rho_i\dot{\theta}_i \end{bmatrix} = &\begin{bmatrix} -\cos\alpha_i & \sin\alpha_i \\ -\sin\alpha_i & -\cos\alpha_i \end{bmatrix} \begin{bmatrix} u_i^r \\ v_i^r \end{bmatrix} + \begin{bmatrix} \bar{u}_i \\ \bar{v}_i \end{bmatrix} \\ &- \begin{bmatrix} \cos\theta_i & \sin\theta_i \\ -\sin\theta_i & \cos\theta_i \end{bmatrix} \begin{bmatrix} v_x^d \\ v_y^d \end{bmatrix} \end{aligned} \tag{18}$$

with $\bar{u}_i := -\cos\alpha_i\widetilde{u}_i + \sin\alpha_i\widetilde{v}_i$ and $\bar{v}_i := -\sin\alpha_i\widetilde{u}_i - \cos\alpha_i\widetilde{v}_i$.

This article has been accepted for publication in a future issue of this journal, but has not been fully edited. Content may change prior to final publication. Citation information: DOI 10.1109/TIE.2021.3076719, IEEE Transactions on Industrial Electronics

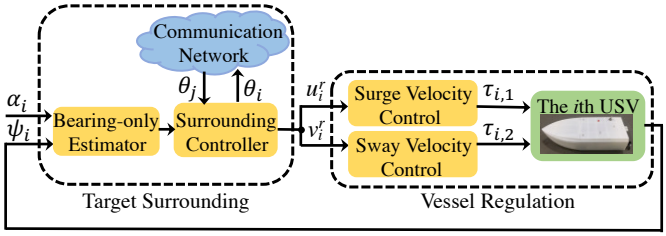

Fig. 3. Closed-loop structure of the bearing-only target-surrounding controller for multi-USV systems.

Now, it is ready to introduce the two main problems addressed in this paper.

Problem 1: (Target surrounding) Design an upper level surrounding signal

$$\{u_i^r, v_i^r\} := f(\alpha_i, \theta_i, \theta_j), j \in \mathcal{N}_i \tag{19}$$

for the multi-USV system composed of (1), (3), (18) to attain the motional target-surrounding (see Definition 1), subject to $\widetilde{u}_i, \widetilde{v}_i$ approaching to zero.

Problem 2: (Vessel Regulation) Design an actuator input

$$\{\tau_1, \tau_2\} := f(u^r, v^r, u, v, r) \tag{20}$$

for a single vessel (2) by ignoring the subscript "i" such that u, v achieve the upper level signals u^r, v^r in Problem 1, i.e., $\lim_{t\to\infty} \widetilde{u}(t) = 0$ and $\lim_{t\to\infty} \widetilde{v}(t) = 0$.

III. Main Results

In this section, Problems 1 and 2 will be technically addressed, as is illustrated in Fig. 3.

A. Target surrounding Control

Let $q_{d,i}$ be the relative position between the USV i and the target vessel as

$$q_{d,i} := q_d - q_i \tag{21}$$

with q_i, q_d given in Eqs. (1) and (3), respectively.

Since the position $q_{d,i}$ and velocity p_d of the target are not available, $\widehat{q}_{d,i}$ and $\widehat{p}_{d,i} = [\widehat{v}_x, \widehat{v}_y]^\intercal$ are defined as the estimates of the $q_{d,i}$ and p_d, respectively, which are designed via the bearing-only measurements as

$$\begin{aligned}\dot{\widehat{q}}_{d,i}(t) =& -\dot{q}_i(t) - c_1(I - \sigma_i(t)\sigma_i(t)^\intercal)\widehat{q}_{d,i}(t) \\ & - c_2\int_0^t (I - \sigma_i(\epsilon)\sigma_i(\epsilon)^\intercal)\widehat{q}_{d,i}(\epsilon)d\epsilon, \\ \dot{\widehat{p}}_{d,i}(t) =& -c_2(I - \sigma_i(t)\sigma_i(t)^\intercal)\widehat{q}_{d,i}(t)dt,\end{aligned} \tag{22}$$

where $c_1, c_2 \in \mathbb{R}^+$ are the estimated gains and σ_i is given Eq. (4). A distributed bearing-only controller is accordingly proposed as below,

$$\begin{bmatrix} u_i^r \\ v_i^r \end{bmatrix} = \begin{bmatrix} -\cos\alpha_i & -\sin\alpha_i \\ \sin\alpha_i & -\cos\alpha_i \end{bmatrix} \times \begin{bmatrix} c_3(\rho_d - \widehat{\rho}_i) + \cos\theta_i\widehat{v}_x + \sin\theta_i\widehat{v}_y \\ c_4(\varsigma_i - \varsigma_{i^-}) + \beta - \sin\theta_i\widehat{v}_x + \cos\theta_i\widehat{v}_y \end{bmatrix}, \tag{23}$$

where $c_3, c_4 \in \mathbb{R}^+$ are the control gains of the USV i, ρ_d is the desired radius in Definition 1, $\widehat{\rho}_i := \|\widehat{q}_{d,i}\|$ denotes the estimated radius in Eq. (22), and ς_i, ς_{i^-} are the separation angles of the USV i and its next-neighbor i^-, respectively.

Remark 1. *Distinct from the target information merely available to partial agents (see, e.g., position-based target-surrounding controllers [20]–[22]), the bearing information σ_i between the USV i and the target vessel is available to each USV in the paper, which forms an ingredient of the bearing-only target estimator* (22)*. The underlying reason lies in that, σ_i is only measured and available to each USV in its respective coordinate and could not be transferred among USVs directly, which is a well accepted assumption in most bearing-only works (see, e.g., [33]–[35]).*

Before giving the main technical result, it is necessary to introduce the following lemmas.

Lemma 1. *[35] A perturbed system is governed by*

$$\dot{x} = A(t, d(t))x + h(t), \tag{24}$$

where $x \in \mathbb{R}^n, h(t) \in \mathbb{R}^n$, $d(t) \in \mathcal{D}$ is a time varying function, and $A : \mathbb{R}^+ \times \mathcal{D} \mapsto \mathbb{R}^{n\times n}$ a continuous and globally bounded function. Then, one has

$$\lim_{t\to\infty} x(t) = 0,$$

if the nominal system $\dot{x} = A(t, d(t))x$ is uniformly globally exponentially stable and $h(t)$ is bounded which satisfies $\lim_{t\to\infty} h(t) = 0$.

Lemma 2. *[38] For a connected and symmetric matrix $L \in \mathbb{R}^{n\times n}$, the following property holds:*

$$\min_{\mathbf{1}^\intercal x = 0, x\neq 0} \frac{x^\intercal L x}{\|x\|^2} \geq \lambda_2(L) > 0. \tag{25}$$

Lemma 3. *[35] For a nominal system governed by*

$$\dot{\widetilde{q}}_{d,i} = -\bar{\sigma}_i\bar{\sigma}_i^\intercal\widetilde{q}_{d,i}, \tag{26}$$

where $\widetilde{q}_{d,i} := \widehat{q}_{d,i} - q_{d,i} \in \mathbb{R}^2$ is the estimated error given in (29)*, and $\bar{\sigma}_i, i \in \mathcal{V}$, denotes a unit vector perpendicular to σ_i with angle $\angle\bar{\sigma}_i = \psi_i + \alpha_i - \pi/2$ in Fig. 1. Then, it derives that*

$$\lim_{t\to\infty} \widetilde{q}_{d,i}(t) = 0,$$

i.e., $\bar{\sigma}_i(t), i \in \mathcal{V}$, is persistently exciting [39], if β in (23) *satisfies*

$$\beta > 2\pi c_4 + p_d^* + \beta^* \tag{27}$$

with a constant $\beta^* \in \mathbb{R}^+$ and the control gain $c_4 \in \mathbb{R}^+$ in the controller (23)*.*

Lemma 4. *For the estimator of the state $q_{d,i}, p_d$ governed by* (1)*,* (3)*,* (21)*,* (22)*, one has*

$$\lim_{t\to\infty} \widehat{q}_{d,i}(t) = q_{d,i}, \lim_{t\to\infty} \widehat{p}_{d,i}(t) = p_d, \tag{28}$$

if β in (23) *satisfies the condition* (27) *in Lemma 3.*

Proof. Let $\widetilde{q}_{d,i}, \widetilde{p}_d$ be the estimated errors as

$$\widetilde{q}_{d,i} := \widehat{q}_{d,i} - q_{d,i}, \ \widetilde{p}_{d,i} := \widehat{p}_{d,i} - p_d. \tag{29}$$

Then, one has

$$\dot{\widetilde{q}}_{d,i} = \dot{\widehat{q}}_{d,i} - \dot{q}_{d,i},\ \dot{\widetilde{p}}_{d,i} = \dot{\widehat{p}}_{d,i}. \tag{30}$$

Substituting Eqs. (3), (22) into Eq. (30) yields

$$\begin{aligned}\dot{\widetilde{q}}_{d,i} =& - c_1(I - \sigma_i\sigma_i^{\intercal})(\widetilde{q}_{d,i} + q_{d,i}) + \widetilde{p}_{d,i},\\ \dot{\widetilde{p}}_{d,i} =& - c_2(I - \sigma_i\sigma_i^{\intercal})(\widetilde{q}_{d,i} + q_{d,i}).\end{aligned} \tag{31}$$

Bearing in mind of the fact that $(I - \sigma_i\sigma_i^{\intercal})q_{d,i} = q_{d,i} - \frac{q_{d,i}}{\|q_{d,i}\|}\frac{q_{d,i}^{\intercal}}{\|q_{d,i}\|}q_{d,i} = 0$ and $\bar{\sigma}_i\bar{\sigma}_i^{\intercal} = I - \sigma_i\sigma_i^{\intercal}$, one has

$$\begin{bmatrix}\dot{\widetilde{q}}_{d,i}\\ \dot{\widetilde{p}}_{d}\end{bmatrix} = A\begin{bmatrix}\dot{\widetilde{q}}_{d,i}\\ \dot{\widetilde{p}}_{d}\end{bmatrix} \tag{32}$$

with

$$A = \begin{bmatrix}-c_1\bar{\sigma}_i\bar{\sigma}_i^{\intercal} & I\\ -c_2\bar{\sigma}_i\bar{\sigma}_i^{\intercal} & 0\end{bmatrix}. \tag{33}$$

Here, $\bar{\sigma}_i$ denotes the unit vector perpendicular to σ_i with angle $\angle\bar{\sigma}_i = \psi_i + \alpha_i - \frac{\pi}{2}$ in Fig. 1. It is clear that the error dynamic (32) converges if the matrix A is Hurwitz, which is equivalent to proving that $\bar{\sigma}_i, i \in \mathcal{V}$, is persistently exciting [39].

In accordance to Lemma 3, one concludes that $\bar{\sigma}_i$ is persistently exciting with a properly chosen β in (27). Accordingly, the estimated errors $\widetilde{q}_{d,i}, \widetilde{p}_{d,i}$ converge, i.e.,

$$\lim_{t\to\infty}\widetilde{q}_{d,i}(t) = 0, \lim_{t\to\infty}\widetilde{p}_{d,i}(t) = 0, \tag{34}$$

the proof is thus completed. □

Remark 2. *The condition $\beta > 2\pi c_4 + p_d^* + \beta^*$ in Eq.* (27) *explicitly shows that all the USVs everlastingly rotate around a motional target vessel under the proposed bearing-only protocol* (23)*, which guarantees that $\bar{\sigma}_i(t), i \in \mathcal{V}$ in* (32) *is persistently exciting and thus forms a necessary condition for the convergence of the estimator* (22) *in Lemma 4. It is different from the traditional surrounding works where the agents just maintain fixed relative displacements around the motional target (see, e.g., [17], [18], [26]).*

Remark 3. *Since the parameter c_4 in* (27) *is a designed control gain of the controller* (23) *and $\beta^* \in \mathbb{R}^+$ a designed constant, the parameter β could be set in prior to satisfy the condition* (27) *and thus all the parameters are guaranteed in practice. To relax the reliance on the global information p_d^*, the estimator gain β can be obtained via over-estimation of $\widehat{p}_d^*$. In other words, specify a number $\widehat{p}_d^* > p_d^*$ for each USV in advance, then β can be selected in the condition $\beta > 2\pi c_4 + \widehat{p}_d^* + \beta^*$ without any global information $p_d^* < \widehat{p}_d^*$. Moreover, the controller* (23) *is implemented distributedly due to the fact that all the parameters in condition (27) could be designed in prior before implementing the individual control law.*

Now, we are ready to present the main technical result.

Theorem 1. *Under Assumptions 1-2, the closed-loop system composed of* (1)*,* (3)*,* (22)*,* (23) *solves Problem 1 subject to* $\lim_{t\to\infty}\widetilde{u}_i(t) = 0,\ \lim_{t\to\infty}\widetilde{v}_i(t) = 0$.

Proof. First, substituting the controller (23) into the closed-loop system (18) yields

$$\begin{aligned}\begin{bmatrix}\dot{\rho}_i\\ \rho_i\dot{\theta}_i\end{bmatrix} =& \begin{bmatrix}c_3(\rho_d - \widehat{\rho}_i) + \cos\theta_i\widehat{v}_x + \sin\theta_i\widehat{v}_y\\ c_4(\varsigma_i - \varsigma_{i^-}) + \beta - \sin\theta_i\widehat{v}_x + \cos\theta_i\widehat{v}_y\end{bmatrix}\\ &+ \begin{bmatrix}\bar{u}_i\\ \bar{v}_i\end{bmatrix} - \begin{bmatrix}\cos\theta_i & \sin\theta_i\\ -\sin\theta_i & \cos\theta_i\end{bmatrix}\begin{bmatrix}v_x^d\\ v_y^d\end{bmatrix}\\ =& \begin{bmatrix}c_3(\rho_d - \widehat{\rho}_i) + \eta_i\\ c_4(\varsigma_i - \varsigma_{i^-}) + \beta + \omega_i\end{bmatrix}\end{aligned} \tag{35}$$

with

$$\begin{aligned}\eta_i =& \bar{u}_i + \cos\theta_i(\widehat{v}_x - v_x^d) + \sin\theta_i(\widehat{v}_y - v_y^d),\\ \omega_i =& \bar{v}_i - \sin\theta_i(\widehat{v}_x - v_x^d) + \cos\theta_i(\widehat{v}_y - v_y^d).\end{aligned}$$

Then, the closed-loop system can be decoupled as

$$\begin{aligned}\dot{\rho}_i =& c_3(\rho_d - \widehat{\rho}_i) + \eta_i,\\ \dot{\theta}_i =& \frac{c_4(\varsigma_i - \varsigma_{i^-}) + \beta}{\rho_i} + \frac{\omega_i}{\rho_i}.\end{aligned} \tag{36}$$

As $\lim_{t\to\infty}\widetilde{u}_i(t) = 0,\ \lim_{t\to\infty}\widetilde{v}_i(t) = 0$, it follows from (18) that

$$\lim_{t\to\infty}\bar{u}_i(t) = 0,\ \lim_{t\to\infty}\bar{v}_i(t) = 0. \tag{37}$$

Moreover, in accordance to Lemma 4, it follows from (3) that

$$\lim_{t\to\infty}\widehat{v}_x(t) - v_x^d = 0,\ \lim_{t\to\infty}\widehat{v}_y(t) - v_y^d = 0. \tag{38}$$

Combining Eqs. (37), (38) and η_i, ω_i in Eq. (35) together yields that

$$\lim_{t\to\infty}\eta_i(t) = 0,\ \lim_{t\to\infty}\omega_i(t) = 0. \tag{39}$$

Let $\widetilde{\rho}_i := \rho_i - \rho_d$ be the radius error, take the temporal derivative of $\widetilde{\rho}_i$ along the trajectory of (36)

$$\begin{aligned}\dot{\widetilde{\rho}}_i =& c_3(\rho_d - \rho_i) + c_3(\rho_i - \widehat{\rho}_i) + \eta_i\\ =& - c_3\widetilde{\rho}_i + \bar{\eta}_i\end{aligned} \tag{40}$$

with $\bar{\eta}_i = c_3(\rho_i - \widehat{\rho}_i) + \eta_i$. Considering the estimated $\widehat{q}_{d,i}$ and $\widehat{p}_d$ in Lemma 4, one has

$$\lim_{t\to\infty}\widehat{\rho}_i(t) = \|\widehat{q}_{d,i}(t)\| = \rho_i(t), \tag{41}$$

it thus follows from Eqs. (39) and (41) that $\lim_{t\to\infty}\bar{\eta}_i(t) = 0$. Rewrite Eq. (36) in a compact form as

$$\dot{\widetilde{\rho}} = -c_3\widetilde{\rho} + \bar{\eta}, \tag{42}$$

with $\widetilde{\rho} = [\widetilde{\rho}_1, \widetilde{\rho}_2, \ldots, \widetilde{\rho}_n]^{\intercal}$ and $\bar{\eta} = [\bar{\eta}_1, \bar{\eta}_2, \ldots, \bar{\eta}_n]^{\intercal} \in \mathbb{R}^n$. Pick a Lyapunov function $V(\widetilde{\rho}) = \frac{1}{2}\widetilde{\rho}^{\intercal}\widetilde{\rho}$, satisfying

$$\begin{aligned}\dot{V}(\widetilde{\rho}) &= -c_3\widetilde{\rho}^{\intercal}\widetilde{\rho} + \widetilde{\rho}^{\intercal}\bar{\eta}\\ &\leq -(1 - m_1)c_3\|\widetilde{\rho}\|^2\\ &\quad +\|\widetilde{\rho}\|(\|\bar{\eta}\| - m_1c_3\|\widetilde{\rho}\|)\end{aligned} \tag{43}$$

with $m_1 \in (0, 1)$. Then, one has

$$\dot{V}(\widetilde{\rho}) \leq -(1 - m_1)c_3\|\widetilde{\rho}\|^2,$$

if $\|\widetilde{\rho}\| \geq \|\bar{\eta}\|/(m_1c_3)$. If $\|\widetilde{\rho}(0)\| \geq \|\bar{\eta}(0)\|/(m_1c_3)$, then $\dot{V}(\widetilde{\rho}) \leq 0$, which implies that $\|\widetilde{\rho}(t)\|$ converges into the ball of radius $\|\bar{\eta}\|/(m_1c_3)$. Otherwise, or, $\|\widetilde{\rho}(0)\| < \|\bar{\eta}(0)\|/(m_1c_3)$, it is clear that $\|\widetilde{\rho}(0)\|$ has already been in the ball of radius

This article has been accepted for publication in a future issue of this journal, but has not been fully edited. Content may change prior to final publication. Citation information: DOI 10.1109/TIE.2021.3076719, IEEE Transactions on Industrial Electronics

$\|\bar{\eta}\|/(m_1c_3)$. Both cases satisfy the definition of input-to-state stability (ISS) [24], which implies that for arbitrary $\|\widetilde{\rho}(0)\|$, $\dot{V}(\widetilde{\rho}) \leq 0$. Accordingly, the closed-loop system (42) is ISS with respect to $\|\bar{\eta}\|$ that satisfies

$$\|\widetilde{\rho}(t)\| \leq \beta(\|\widetilde{\rho}(0\|,t)) + \gamma\big(\sup_{0\leq\tau\leq t}\|\bar{\eta}(\tau)\|\big), \forall t>0, \tag{44}$$

where $\beta(\cdot)$ is a $\mathcal{KL}$ function with $\kappa_1 = 1/(m_1c_3)$ being the system gain (see [40]). Due to the fact that $\lim_{t\to\infty}\bar{\eta}_i(t) = 0$ and the $\mathcal{KL}$ function satisfies $\lim_{t\to\infty}\beta((\|\widetilde{\rho}\|,t)) = 0$, it follows that $\lim_{t\to\infty}\widetilde{\rho}(t) = 0$ in Eq. (44).

In what follows, we will prove the even phase distribution of all the USVs around the motional target vessel.

Recall the definition of ς_i in (7), it follows from (36) that

$$\begin{aligned}\dot{\varsigma}_i =&\dot{\theta}_{i^+} - \dot{\theta}_i\\ =&\frac{c_4(\varsigma_{i^+}-\varsigma_i)+\beta}{\rho_{i^+}} - \frac{c_4(\varsigma_i-\varsigma_{i^-})+\beta}{\rho_i}\\ &+\frac{\omega_{i^+}}{\rho_{i^+}} - \frac{\omega_i}{\rho_i}\\ =&\frac{c_4(\varsigma_{i^+}-2\varsigma_i+\varsigma_i)}{\rho_d} + \frac{c_4}{\rho_d}\epsilon_i + \varpi_i,\end{aligned} \tag{45}$$

where i^+, i^- denotes the pre-neighbor and next-neighbor of the USV i, respectively, and

$$\begin{aligned}\epsilon_i :=&\frac{(\varsigma_{i^+}-\varsigma_i)(\rho_{i^+}-\rho_d)}{\rho_{i^+}} - \frac{(\varsigma_i-\varsigma_{i^-})(\rho_i-\rho_d)}{\rho_i},\\ \varpi_i :=&\frac{\beta(\rho_{i^+}-\rho_i)}{\rho_i\rho_{i^+}} + \frac{\omega_{i^+}\rho_i - \omega_i\rho_{i^+}}{\rho_i\rho_{i^+}}.\end{aligned} \tag{46}$$

Rewrite (45) in a compact form as

$$\dot{\varsigma} = -\frac{c_4}{\rho_d}L(\mathcal{V})\varsigma + \frac{c_4}{\rho_d}\epsilon + \varpi \tag{47}$$

with $\varsigma = [\varsigma_1,\varsigma_2,\ldots,\varsigma_n]^\intercal$, $\epsilon = [\epsilon_1,\epsilon_2,\ldots,\epsilon_n]^\intercal$, $\varpi = [\varpi_1,\varpi_2,\ldots,\varpi_n]^\intercal$ and a Laplacian matrix $L(\mathcal{V}) \in \mathbb{R}^{n\times n}$ corresponding to the strongly connected graph $\mathcal{G}(\mathcal{V},\mathcal{E})$.

Let $\widetilde{\varsigma} = [\widetilde{\varsigma}_1,\widetilde{\varsigma}_2,\ldots,\widetilde{\varsigma}_n]^\intercal \in \mathbb{R}^n$ be the error vector between the separation angles and the desired angles as

$$\widetilde{\varsigma} = \mathbf{1}\otimes\frac{2\pi}{n} - \varsigma \tag{48}$$

with a vector $\mathbf{1}\in\mathbb{R}^n$, it follows from Eqs. (47) and (48) that

$$\begin{aligned}\dot{\widetilde{\varsigma}} =&\frac{c_4}{\rho_d}L(\mathcal{V})\varsigma + \frac{c_4}{\rho_d}\epsilon + \varpi\\ =&\frac{c_4}{\rho_d}L(\mathcal{V})\left(\mathbf{1}\otimes\frac{2\pi}{n} - \widetilde{\varsigma}\right) + \frac{c_4}{\rho_d}\epsilon + \varpi.\end{aligned} \tag{49}$$

It is worth mentioning that ϵ_i, ϖ_i can be formulated as

$$\epsilon_i := \frac{(\widetilde{\varsigma}_i - \widetilde{\varsigma}_{i^+})(\rho_{i^+}-\rho_d)}{\rho_{i^+}} - \frac{(\widetilde{\varsigma}_{i^-} - \widetilde{\varsigma}_i)(\rho_i-\rho_d)}{\rho_i}. \tag{50}$$

Since the matrix $L(\mathcal{V})$ satisfies $L(\mathcal{V})\mathbf{1} = \mathbf{0}$, the dynamic of $\dot{\widetilde{\varsigma}}$ in (49) writes

$$\dot{\widetilde{\varsigma}} = -\frac{c_4}{\rho_d}L(\mathcal{V})\widetilde{\varsigma} + \frac{c_4}{\rho_d}\epsilon + \varpi. \tag{51}$$

Meanwhile, it follows from Eq. (44) that

$$\rho_i(t) \geq \rho_d - \beta(\|\widetilde{\rho}(0\|,t)) - \gamma\big(\sup_{0\leq\tau\leq t}\|\bar{\eta}(\tau)\|\big). \tag{52}$$

Due to the fact that $\beta(\|\widetilde{\rho}(0\|,t)) > 0$, $\gamma\big(\sup\|\bar{\eta}(\tau)\|\big) > 0$ satisfies $\lim_{t\to\infty}\beta((\|\widetilde{\rho}\|,t)) = 0$ and $\lim_{t\to\infty}\bar{\eta}_i(t) = 0$, which implies that there exists $t_1 > 0$ such that $\rho_i(t) > \bar{\rho}, i\in\mathcal{V}, t > t_1$ with a constant $\bar{\rho} > 0$ and $\rho_d > 0$. From the fact that $\widetilde{\varsigma}_i - \widetilde{\varsigma}_{i^+} \leq 2\pi, i\in\mathcal{V}$, it follows from Eqs. (46) and (50) that

$$\begin{aligned}\|\epsilon_i\| \leq&\frac{2\pi|\rho_{i^+}-\rho_d|}{\bar{\rho}} + \frac{2\pi|\rho_i-\rho_d|}{\bar{\rho}},\\ \|\varpi_i\| \leq&\frac{\beta|\rho_{i^+}-\rho_i|}{\bar{\rho}^2} + \frac{\omega_{i^+}}{\bar{\rho}} + \frac{\omega_i}{\bar{\rho}},\end{aligned} \tag{53}$$

which implies that $\|\epsilon_i\|, \|\varpi_i\|$ are both bounded. Moreover, it follows from Eqs. (39) and (44) that $\lim_{t\to\infty}\|\epsilon_i\| = 0, \lim_{t\to\infty}\|\varpi_i\| = 0$, which implies that

$$\lim_{t\to\infty}\frac{c_4}{\rho_d}\|\epsilon(t)\| + \|\varpi(t)\| = \mathbf{0} \tag{54}$$

with a zero vector $\mathbf{0}\in\mathbb{R}^n$. Consider a nominal system of (51) as

$$\dot{\widetilde{\varsigma}} = -\frac{c_4}{\rho_d}L(\mathcal{V})\widetilde{\varsigma}. \tag{55}$$

As $\mathcal{G}(\mathcal{V},\mathcal{E})$ is time changing during the target surrounding mission, pick a Lyapunov candidate as follows,

$$V(\widetilde{\varsigma}) = \frac{1}{2}\widetilde{\varsigma}^\intercal\widetilde{\varsigma}, \tag{56}$$

which is piecewisely continuously differentiable. Then, when the topology $\mathcal{G}(\mathcal{V},\mathcal{E})$ remains unchanged, the corresponding $L(\mathcal{V})$ is symmetric and strongly connected. Take the right upper Dini temporal derivative of $V(\widetilde{\varsigma})$ (see [19]) along the trajectory of (55), one has

$$D^+V(\widetilde{\varsigma}) = \frac{1}{2}(\widetilde{\varsigma}^\intercal\dot{\widetilde{\varsigma}} + \dot{\widetilde{\varsigma}}^\intercal\widetilde{\varsigma}) = -\frac{c_4}{\rho_d}\widetilde{\varsigma}^\intercal L(\mathcal{V})\widetilde{\varsigma}^\intercal. \tag{57}$$

Bearing in mind of $\mathbf{1}^\intercal\widetilde{\varsigma} = 2\pi - \mathbf{1}^\intercal\varsigma = 2\pi - 2\pi = 0$, $\varsigma \neq \mathbf{0}$ and Eqs. (7) and (48), it follows from Lemma 2 that

$$\frac{dV(\widetilde{\varsigma})}{dt} \leq -\frac{c_4}{\rho_d}\lambda_2(L(\mathcal{V}))\|\widetilde{\varsigma}\|^2. \tag{58}$$

According to the minimal-neighbor strategy in Assumption 2, the graph $\mathcal{G}(\mathcal{V},\mathcal{E})$ belongs to a finite set. Moreover, there exists a lower bound $\chi > 0$ satisfying $\lambda_2(L(\mathcal{V})) > \chi$, which implies that

$$\frac{dV(\widetilde{\varsigma})}{dt} \leq -\frac{c_4}{\rho_d}\chi\|\widetilde{\varsigma}\|^2 \leq 0, \forall t > t_1. \tag{59}$$

Then, $\widetilde{\varsigma}$ in the nominal system (55) satisfies $\lim_{t\to\infty}\widetilde{\varsigma}_i(t) = 0$, exponentially.

In accordance to Lemma 1 and (54), it can be deduced that the perturbed system (51) satisfies that $\lim_{t\to\infty}\widetilde{\varsigma}(t) = 0$, i.e., $\lim_{t\to\infty}\varsigma_i(t) = 2\pi/n$ in (8) or the phase distribution becomes even. The proof is thus completed. □

Remark 4. *In the aforementioned bearing-only frameworks [33]–[35], the target velocity is mostly assumed to be available to a small partial of the agents. However, the proposed estimator* (22) *utilized the bearing-only information of the motional target vessel without any needness for the target velocity, which is less costly as bearings are generally cheaper than velocity sensors.*

B. Vessel Regulation Control

Upon achieving the target surrounding mission of multi-USV systems with upper level signals u_i^r, v_i^r subject to $\widetilde{u}_i, \widetilde{v}_i$ approaching zero, we are ready to tackle Problem 2, that is, to design the actuator inputs $\tau_{i,1}, \tau_{i,2}$ for the USV i with the dynamic system (2) such that u_i, v_i approach to u_i^r, v_i^r, respectively.

With the $\widetilde{u}_i, \widetilde{v}_i$ in Eq. (17), the actuator inputs $\tau_{i,1}, \tau_{i,2}$ for USV i are thus designed as

$$\begin{aligned}\tau_{i,1} =&\frac{1}{k_3 u_i^r}(\dot{u}_i^r u_i - k_1 u_i^r u_i - k_2 u_i^r v_i r_i - c_1 u_i \widetilde{u}_i),\\ \tau_{i,2} =&\frac{1}{k_5}(-k_4 r_i - c_3 \widetilde{r}_i + \dot{r}_i^r),\end{aligned} \tag{60}$$

where $c_1, c_2, c_3 \in \mathbb{R}^+$ are positive parameters to be designed afterwards, $\widetilde{r}_i$ and r_i^r the yaw velocity error and the desired yaw velocity, respectively, to be formulated as

$$\begin{aligned}\widetilde{r}_i =& r_i - \widetilde{r}_i^r,\\ r_i^r =&\frac{1}{k_7 u_i}(-k_6 v_i + \dot{v}_i^r - c_2 \widetilde{v}_i).\end{aligned} \tag{61}$$

Theorem 2. *For the designed signals u_i^r, v_i^r, a USV dynamic system composed of* (2) *and* (60) *achieves $\lim_{t\to\infty} \widetilde{u}_i(t) = 0$, $\lim_{t\to\infty} \widetilde{v}_i(t) = 0$ or solves Problem 2 only if $u_i(0) > 0$.*

Proof. It follows from the definition $\widetilde{u}_i$ in (17) and the dynamic $\dot{u}_i$ in (2) that

$$\dot{\widetilde{u}}_i = k_1 u_i + k_2 v_i r_i + k_3 \tau_{i,1} - \dot{u}_i^r, \tag{62}$$

Substituting $\tau_{i,1}$ in Eq. (60) into Eq. (62) yields

$$\begin{aligned}\dot{\widetilde{u}}_i =&k_1 u_i + k_2 v_i r_i + k_3(\frac{1}{k_3 u_i^r}(\dot{u}_i^r u_i - k_1 u_i^r u_i\\ &- k_2 u_i^r v_i r_i - c_1 u_i \widetilde{u}_i)) - \dot{u}_i^r,\\ =&\frac{\dot{u}_i^r u_i - \dot{u}_i^r u_i^r - c_1 u_i \widetilde{u}_i}{u_i^r}.\end{aligned} \tag{63}$$

According to the definitions of non-autonomous and autonomous system [24], the closed-loop system (63) is time invarirant, which implies that the system (63) is an autonomous system.

Pick a Lyapunov function candidate as

$$V(u_i, u_i^r) = \left(\frac{u_i - u_i^r}{u_i}\right)^2, \tag{64}$$

whose temporal derivative along the trajectory of (63) is

$$\begin{aligned}\dot{V}(u_i, u_i^r) =&\frac{2\widetilde{u}_i u_i^2(\dot{u}_i - \dot{u}_i^r) - 2\widetilde{u}_i^2 u_i \dot{u}_i}{u_i^4}\\ =&-\frac{2c_1\widetilde{u}_i^2}{u_i^2} \le 0.\end{aligned} \tag{65}$$

It is derived that $\dot{V}(u_i, u_i^r) = 0$ only if $\widetilde{u}_i = 0$, which implies the largest invariance set in $\{u_i | \dot{V}(u_i, u_i^r) = 0\}$ only contains one point $\{u_i^r\}$, and hence the invariance set is compact (bounded closed set). In accordance to the LaSalle's invariance principle [24], the trajectory of u_i converges to u_i^r, i.e., $\lim_{t\to\infty} \widetilde{u}_i(t) = 0$.

Moreover, it is deduced that $V(u_i, u_i^r)$ is bounded as well. The condition $u_i(0) > 0$ given in Theorem 2 implies that $u_i(t) > 0$, which formulates r_i^r in the next proof of $\lim_{t\to\infty} \widetilde{v}_i(t) = 0$.

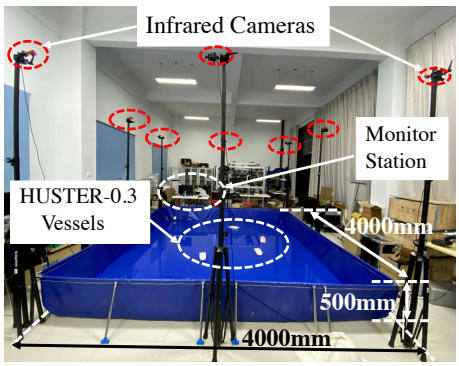

Fig. 4. The real map of the indoor multi-USV platform.

Substituting the desired yaw velocity r_i^r in Eq. (61) into the dynamic $\dot{v}_i$ in (2) yields

$$\begin{aligned}\dot{\widetilde{v}}_i =&k_6 v_i + k_7 u_i r_i^r + k_7 u_i \widetilde{r}_i - \dot{v}_i^r\\ =&-c_2 \widetilde{v}_i + k_7 u_i \widetilde{r}_i.\end{aligned} \tag{66}$$

It follows from the dynamic $\dot{r}_i$ in (2) that the derivative of $\widetilde{r}_i$ in (61) is,

$$\dot{\widetilde{r}}_i = k_4 r_i + k_5 \tau_{i,2} - \dot{r}_i^r. \tag{67}$$

Analogously, it follows from Eqs. (60) and (67) that

$$\begin{aligned}\dot{\widetilde{r}}_i =&k_4 r_i + k_5(\frac{1}{k_5}(-k_4 r_i - c_3 \widetilde{r}_i + \dot{r}_i^r)) - \dot{r}_i^r\\ =&-c_3 \widetilde{r}_i,\end{aligned} \tag{68}$$

which implies that $\lim_{t\to\infty} \widetilde{r}_i(t) = 0$ exponentially.

Due to the upper level signals u_i^r, v_i^r and the signal error $\widetilde{u}_i$ are all bounded, one has u_i is bounded, which implies that $\lim_{t\to\infty} k_7 u_i \widetilde{r}_i(t) = 0$. Considering the dynamic of $\widetilde{v}_i$ in Eq. (66), one can conclude that $\lim_{t\to\infty} \widetilde{v}_i(t) = 0$ exponentially, which completes the proof. □

Remark 5. *The $\tau_{i,1}$ in* (60) *not only plays a role in approaching to u_i^r, but also guarantees $u_i(t) > 0$ if $u_i(0) > 0$, which is a necessary condition for the desired yaw velocity r_i^r in Eq.* (61) *and thus outperforms the existing work [17].*

IV. Experiments

In this section, bearing-only target-surrounding experiments are conducted on our established indoor multi-USV platform, which is composed of a motional capturing system (eight infrared cameras Optitrack Flex 3), a monitor station, three 300mm-long 3D-printed HUSTER-0.3 USVs, a target vessel, and a 4000 mm ×4000 mm ×500mm pool in Fig. 4. Each USV is equipped with two DC motors (5V), two transmission shafts (150mm), two speed encoders (Freescale Mini256ABC), an onboard 2.4GHz wireless components (NRF24L01), three infrared emitters (Peak wavelength: 850nm), two indicators (LED) and an LI-PO Battery (7.4V, 1300mAh, 25c). These instruments are all managed by a micro controller (STM32F103CBT6). Detailed components can be referred [26] with parameter setting.

This article has been accepted for publication in a future issue of this journal, but has not been fully edited. Content may change prior to final publication. Citation information: DOI 10.1109/TIE.2021.3076719, IEEE Transactions on Industrial Electronics

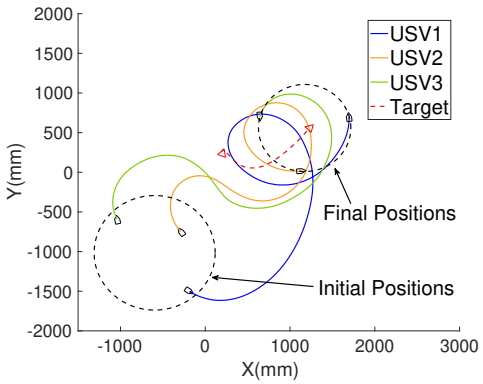

Fig. 5. A bearing-only target surrounding process of a motional target vessel with three USVs, where the colored lines are the moving trajectories of the three USVs whereas the red dashed line is the target vessel's trajectory.

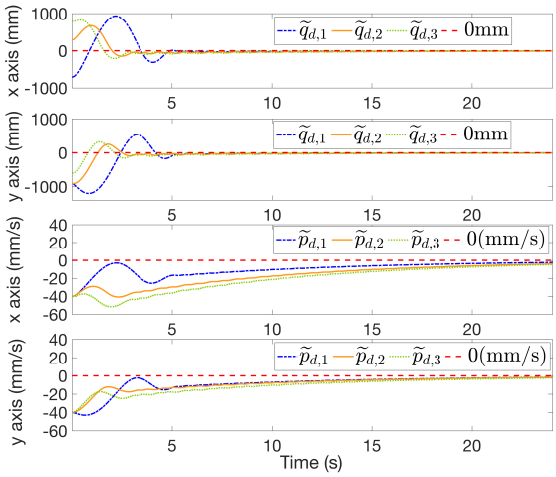

Fig. 6. Temporal evolution of the estimated relative-position errors $\widetilde{q}_{d,i}, i = 1, 2, 3$, and the estimated relative-velocity errors $\widetilde{p}_{d,i}, i = 1, 2, 3$, between the USVs and the target vessel.

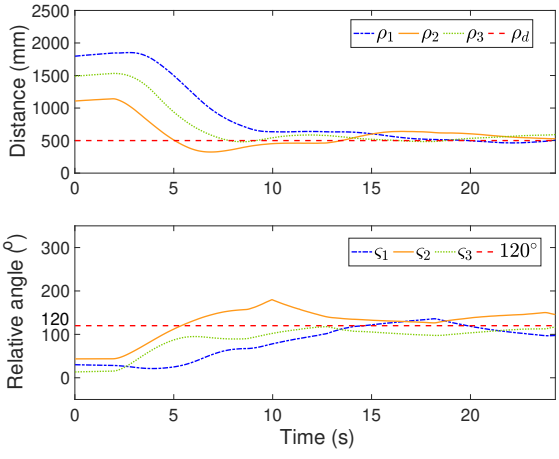

Fig. 7. Temporal evolution of the relative distances $\rho_i, i = 1, 2, 3$, and the separation angles $\varsigma_i, i = 1, 2, 3$.

More concretely, the working principle of the platform is summarized as below. First, by detecting the embedded infrared emitters on each USV with multi-infrared cameras, the motional capturing system calculates the positions and velocities of the USVs with sufficiently high accuracies of $\pm$3mm and $\pm$5mm/s, respectively. Then, with the detected positions and velocities of USVs, the corresponding bearing angle among the target vessel and the USVs can be calculated by the monitor station and then transferred to each USV via 2.4GHz wireless components at 100Hz. Moreover, with calculation of the neighboring bearing angles under Assumption 2, the separation angle of the pre- and next-neighbors could be transferred among USVs via wireless network as well. In this way, each USV estimates the velocity of the target with neighboring bearing angles, which is used to yield its calculated individual control signal to fulfill the motional target surrounding mission.

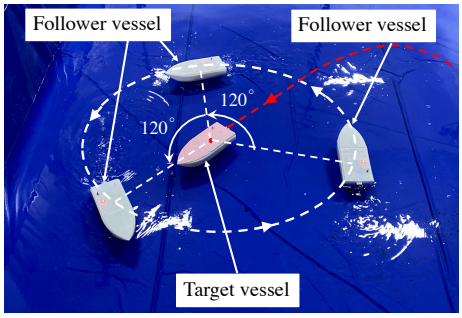

Fig. 8. A snapshot of the target-surrounding mission with a motional target vessel at 24-th second from the start.

In the experiments, the multi-USV system consists of three USVs and a target vessel. By conducting classical zigzag tracking experiments (see, e.g., [17]) and collecting data with the sampling period of 0.1s, the dynamic parameters $k_i, i = 1, 2, \cdots, 7$, in Eq. (2) are identified as $k_1 = 0.9969, k_2 = -0.0731, k_3 = 0.00062, k_4 = 0.2491, k_5 = 0.00014, k_6 = 0.9877$ and $k_7 = 0.0081$ via a least square identification method on Zigzag tracking experimental data. Initially, three USVs are randomly distributed on the pool within an area of $[-1000, 0]$mm $\times$ $[-1500, 0]$mm (the entire pool range is set as $[-1500, 2500]$mm $\times$ $[-2000, 2000]$mm). The initial velocities of USVs are set as $u_i(0) = 10$ mm/s, $v_i(0) = 0$ mm/s, $r_i(0) = 0$ rad/s, $i = 1, 2, 3$. The position of the target vessel is set randomly within an area of $[0, 500]$mm $\times$ $[0, 500]$mm and the velocity is set as $p_d = [40, 40]^{\mathrm{T}}$mm/s satisfying $\|p_d\| < p_d^* = 80$mm/s of Assumption 1. The desired radius is set as $\rho_d = 500$ mm. In light of Theorem 1, the parameters of estimator and the controller (23) are set as $c_1 = 1$, $c_2 = 0.01$, $c_3 = 1$ and $c_4 = 1$. With the selected ρ_d and c_4, the parameter β in (23) is set as $\beta = 200$, which satisfies condition (27) with $\beta^* = 20$ as well. The parameters of the actuator inputs in (60) are set as $c_5 = 2$, $c_6 = 1.2$, $c_7 = 2$ according to Theorem 2.

In accordance to surrounding behavior in Theorem 1, Fig. 5 illustrates the surrounding trajectories for a motional target vessel with three USVs. Here, all the USVs surround and rotate evenly around the motional target vessel with bearing-only measurements. Fig. 6 exhibits the convergence procedure of the estimated relative-position errors $\widetilde{q}_{d,i}, i = 1, 2, 3$, and

the estimated relative-velocity errors $\widetilde{p}_{d,i}, i = 1, 2, 3$, between the USVs and the target vessel. As is shown in Fig. 7, the relative distances $\rho_i, i = 1, 2, 3$, finally approach to the prescribed radius $\rho_d = 500$mm with separation angles converging to 120° in less than 30 seconds, showing the achievements of target surrounding in Definition 1. Fig. 8 plots a snapshot of the target-surrounding steady status corresponding to the 24-th second from the start in Fig. 5.

Remark 6. *Due to the limited installation spaces of indoor USVs, the bearing angles could not be detected by the onboard sensors. But for outdoor USVs with sufficiently large sizes, onboard sensors of bearing angles would be available.*

Remark 7. *With the assistance of least square identification on zigzag tracking experimental data with persistently exciting (PE) input signals, the identification errors of vehicle parameters are generally bounded, which could be satisfactorily addressed by the proposed vessel regulation law* (60)*. Moreover, as is illustrated in Fig. 3, a high-level multi-vessel target surrounding control law and a low level single vessel regulation are combined to build up a hierarchical closed-loop system, where the upper level surrounding control signals u_i^r, v_i^r and the low level regulation laws $\tau_{i,1}, \tau_{i,2}$ have inherent robustness against bounded identification errors that is guaranteed by Theorem 1 nourished by input-to-state stable (ISS) theory. Therefore, experiments results show robustness against bounded identification errors (see Figs. 5-8). To endow the multi-USV system with superior robustness to even larger identification errors, one could add terms corresponding to coefficient uncertainties and external noise to the vessel dynamics model* (2)*, and seek assistance from the most recently developed robust formation controllers (see [41]–[43]).*

Remark 8. *The indoor multi-USV experimental platform contains the function of collision avoidance. Once some USV-USV relative distance is smaller than the prescribed safe distance, the involved USV would switch to the safe mode, that is, the rear USV slows down and deviates or even stops to avoid collision avoidance until the USV-USV distance is no less than the safe distance again. Afterwards, the distributed surrounding control laws are switched back to* (23) *and* (60)*. Therein, collision avoidance could be regarded as a disturbance to the closed-loop system. It is still challenging to theoretically prove the motional target surrounding convergence under the aforementioned switching schemes. It can be expected that, when the pool is large enough, each USV will have sufficiently room to conduct the collision-avoidance operation. When the robots are close to a collectively circular motion after a few times of collision avoidance, they will be sufficiently separated and not necessarily switch to the collision avoidance algorithm any longer. Thus, the proposed controllers* (23)*,* (60) *have robustness to deal with the disturbances induced by collision avoidance operations. As a result, the motional target surrounding can still be guaranteed.*

V. Conclusion

In this paper, we have presented a distributed bearing-only controller, such that networked USVs surround a motional target vessel with inter-USV topologies. The virtue of the present scheme lies in upper level calculation of the desirable surge and sway velocities for each USV so as to rotate evenly around the motional target vessel via bearing-only measurements, and single vessel regulation to track the upper level signal. The effectiveness of the controller has been verified via experiments with a real multi-USV platform. Future work will focus on improving the capability of the multi-USV surrounding controller to deal with intermittent bearing-only measurements, communication delay, large identification errors, intensive external wave and tide disturbances, and multiple motional targets.

References

[1] E. Lefeber, K. Y. Pettersen, and H. Nijmeijer, "Tracking control of an underactuated ship," *IEEE Transactions on Control Systems Technology*, vol. 11, no. 1, pp. 52–61, 2003.

[2] H. Ashrafiuon, K. R. Muske, L. C. McNinch, and R. A. Soltan, "Sliding-mode tracking control of surface vessels," *IEEE Transactions on Industrial Electronics*, vol. 55, no. 11, pp. 4004–4012, 2008.

[3] K. Shojaei, "Neural adaptive robust control of underactuated marine surface vehicles with input saturation," *Applied Ocean Research*, vol. 53, pp. 267–278, 2015.

[4] W. He, Z. Yin, and C. Sun, "Adaptive neural network control of a marine vessel with constraints using the asymmetric barrier lyapunov function," *IEEE Transactions on Cybernetics*, vol. 47, no. 7, pp. 1641–1651, 2017.

[5] N. Wang and H. He, "Dynamics-level finite-time fuzzy monocular visual servo of an unmanned surface vehicle," *IEEE Transactions on Industrial Electronics*, vol. 67, no. 11, pp. 9648–9658, 2019.

[6] Z. Peng, J. Wang, and Q.-L. Han, "Path-following control of autonomous underwater vehicles subject to velocity and input constraints via neurodynamic optimization," *IEEE Transactions on Industrial Electronics*, vol. 66, no. 11, pp. 8724–8732, 2018.

[7] B. Liu, H.-T. Zhang, H. Meng, D. Fu, and H. Su, "Scanning-chain formation control for multiple unmanned surface vessels to pass through water channels," *IEEE Transactions on Cybernetics*, in press, doi: 10.1109/TCYB.2020.2997833.

[8] N. Wang, G. Xie, X. Pan, and S.-F. Su, "Full-state regulation control of asymmetric underactuated surface vehicles," *IEEE Transactions on Industrial Electronics*, vol. 66, no. 11, pp. 8741–8750, 2019.

[9] Z. Peng, J. Wang, D. Wang, and Q.-L. Han, "An overview of recent advances in coordinated control of multiple autonomous surface vehicles," *IEEE Transactions on Industrial Informatics*, vol. 17, no. 2, pp. 732–745, 2020.

[10] L. Liu, D. Wang, Z. Peng, T. Li, and C. P. Chen, "Cooperative path following ring-networked under-actuated autonomous surface vehicles: Algorithms and experimental results," *IEEE Transactions on Cybernetics*, vol. 50, no. 4, pp. 1519–1529, 2020.

[11] D. Li, G. Ma, W. He, S. S. Ge, and T. H. Lee, "Cooperative circumnavigation control of networked microsatellites," *IEEE Transactions on Cybernetics*, vol. 50, no. 10, pp. 4550–4555, 2019.

[12] M. Hassan, E. Aljuwaiser, and R. Badr, "A new on-line observer-based controller for leader-follower formation of multiple nonholonomic mobile robots," *Journal of the Franklin Institute*, vol. 355, no. 5, pp. 2436–2472, 2018.

[13] K. Shojaei, "Observer-based neural adaptive formation control of autonomous surface vessels with limited torque," *Robotics and Autonomous Systems*, vol. 78, pp. 83–96, 2016.

[14] Z. Sun, G. Zhang, Y. Lu, and W. Zhang, "Leader-follower formation control of underactuated surface vehicles based on sliding mode control and parameter estimation," *ISA Transactions*, vol. 72, pp. 15–24, 2018.

[15] F. Chen, W. Ren, and Y. Cao, "Surrounding control in cooperative agent networks," *Systems & Control Letters*, vol. 59, no. 11, pp. 704–712, 2010.

[16] Y. Lan, G. Yan, and Z. Lin, "Distributed control of cooperative target enclosing based on reachability and invariance analysis," *Systems & Control Letters*, vol. 59, no. 7, pp. 381–389, 2010.

[17] B. Liu, Z. Chen, H. Zhang, X. Wang, T. Geng, H. Su, and J. Zhao, "Collective dynamics and control for multiple unmanned surface vessels," *IEEE Transactions on Control Systems Technology*, vol. 28, no. 6, pp. 2540–2547, 2020.

[18] Z. Chen, "A cooperative target-fencing protocol of multiple vehicles," *Automatica*, vol. 107, pp. 591–594, 2019.

[19] J. Guo, G. Yan, and Z. Lin, "Local control strategy for moving-target-enclosing under dynamically changing network topology," *Systems & Control Letters*, vol. 59, no. 10, pp. 654–661, 2010.

[20] X. Yu and L. Liu, "Distributed circular formation control of ring-networked nonholonomic vehicles," *Automatica*, vol. 68, pp. 92–99, 2016.

[21] ——, "Cooperative control for moving-target circular formation of nonholonomic vehicles," *IEEE Transactions on Automatic Control*, vol. 62, no. 7, pp. 3448–3454, 2017.

[22] S. Shoja, M. Baradarannia, F. Hashemzadeh, M. Badamchizadeh, and P. Bagheri, "Surrounding control of nonlinear multi-agent systems with non-identical agents," *ISA Transactions*, vol. 70, pp. 219–227, 2017.

[23] Y. Shi, R. Li, and K. L. Teo, "Cooperative enclosing control for multiple moving targets by a group of agents," *International Journal of Control*, vol. 88, no. 1, pp. 80–89, 2015.

[24] H. K. Khalil, *Nonlinear Systems*. Upper Saddle River, 2002.

[25] C. Li, L. Chen, Y. Guo, and Y. Lyu, "Cooperative surrounding control with collision avoidance for networked lagrangian systems," *Journal of the Franklin Institute*, vol. 355, no. 12, pp. 5182–5202, 2018.

[26] B.-B. Hu, H.-T. Zhang, and J. Wang, "Multiple-target surrounding and collision avoidance of a second-order nonlinear multi-agent system," *IEEE Transactions on Industrial Electronics*, in press, doi: 10.1109/TIE.2020.3000092.

[27] Z. Peng, Y. Jiang, and J. Wang, "Event-triggered dynamic surface control of an underactuated autonomous surface vehicle for target enclosing," *IEEE Transactions on Industrial Electronics*, vol. 68, no. 4, pp. 3402–3412, 2020.

[28] X. Jin, "Fault tolerant finite-time leader–follower formation control for autonomous surface vessels with los range and angle constraints," *Automatica*, vol. 68, pp. 228–236, 2016.

[29] B.-B. Hu, H.-T. Zhang, B. Liu, H. Meng, and G. Chen, "Distributed surrounding control of multiple unmanned surface vessels with varying interconnection topologies," *IEEE Transactions on Control Systems Technology*, in press, doi: 10.1109/TCST.2021.3057640.

[30] L. Kou, Y. Huang, Z. Chen, S. He, and J. Xiang, "Cooperative fencing control of multiple second-order vehicles for a moving target with and without velocity measurements," *International Journal of Robust and Nonlinear Control*, in press, doi: 10.1002/rnc.5493.

[31] R. Zheng, Y. Liu, and D. Sun, "Enclosing a target by nonholonomic mobile robots with bearing-only measurements," *Automatica*, vol. 53, pp. 400–407, 2015.

[32] R. Li, Y. Shi, and Y. Song, "Localization and circumnavigation of multiple agents along an unknown target based on bearing-only measurement: A three dimensional solution," *Automatica*, vol. 94, pp. 18–25, 2018.

[33] M. Deghat, I. Shames, B. D. Anderson, and C. Yu, "Localization and circumnavigation of a slowly moving target using bearing measurements," *IEEE Transactions on Automatic Control*, vol. 59, no. 8, pp. 2182–2188, 2014.

[34] Z. Yang, S. Zhu, C. Chen, G. Feng, and X. Guan, "Entrapping a target in an arbitrarily shaped orbit by a single robot using bearing measurements," *Automatica*, vol. 113, p. 108805, 2020.

[35] L. Dou, C. Song, X. Wang, L. Liu, and G. Feng, "Target localization and enclosing control for networked mobile agents with bearing measurements," *Automatica*, vol. 118, p. 109022, 2020.

[36] Y. Jiang, Z. Peng, D. Wang, and C. P. Chen, "Line-of-sight target enclosing of an underactuated autonomous surface vehicle with experiment results," *IEEE Transactions on Industrial Informatics*, vol. 16, no. 2, pp. 832–841, 2019.

[37] T. I. Fossen, *Handbook of Marine Craft Hydrodynamics and Motion Control*. John Wiley & Sons, 2011.

[38] C. Godsil and G. F. Royle, *Algebraic Graph Theory*. Springer Science & Business Media, 2013.

[39] S. Sastry and M. Bodson, *Adaptive Control: Stability, Convergence and Robustness*. Courier Corporation, 2011.

[40] A. Isidori, *Nonlinear Control Systems II*. Springer Science & Business Media, 2012.

[41] H. Liu, Y. Tian, F. L. Lewis, Y. Wan, and K. P. Valavanis, "Robust formation tracking control for multiple quadrotors under aggressive maneuvers," *Automatica*, vol. 105, pp. 179–185, 2019.

[42] B. S. Park and S. J. Yoo, "Connectivity-maintaining and collision-avoiding performance function approach for robust leader–follower formation control of multiple uncertain underactuated surface vessels," *Automatica*, vol. 127, p. 109501, 2021.

[43] Y. Hua, X. Dong, Q. Li, and Z. Ren, "Distributed time-varying formation robust tracking for general linear multiagent systems with parameter uncertainties and external disturbances," *IEEE Transactions on Cybernetics*, vol. 47, no. 8, pp. 1959–1969, 2017.

Bin-Bin Hu received the B.E. degree in electrical engineering and automation from Jiangnan Univeristy, Wuxi, China, in 2017. He is currently working toward the Ph.D. degree in control science and technology at Huazhong University of Science and Technology, Wuhan, China. His research interests include multi-agent systems, and control of unmanned surface vehicles.

Hai-Tao Zhang (M'07–SM'13) received the B.E. and Ph.D. degrees from the University of Science and Technology of China, Hefei, China, in 2000 and 2005, respectively. In 2007, he was a Postdoctoral Researcher with the University of Cambridge, Cambridge, U.K. Since 2005, he has been with the Huazhong University of Science and Technology, Wuhan, China, where he was an Associate Professor from 2005 to 2010, and has been a Full Professor since 2010. He is a Cheung Kong Young Scholar. His research interests include swarming intelligence, model predictive control, and unmanned system cooperation control. He is/was an Associate Editor of *IEEE Transaction on Systems, Man, and Cybernetics: Systems, IEEE Transactions on Circuits and Systems–Part II: Express Briefs, Asian Journal of Control*, IEEE Conference on Decision and Control, and American Control Conference.